Cavity solitons in semiconductor microresonators: Existence, stability, and dynamical properties

T. Maggipinto and M. Brambilla
INFM, Dipartimento di Fisica Interateneo, Universitá e Politecnico di Bari, Via Orabona 4, 70126 Bari, Italy

G. K. Harkness and W. J. Firth
Department of Physics and Applied Physics, University of Strathclyde, 107 Rottenrow, Glasgow G4 0NG, United Kingdom
(Received 12 July 2000)

We apply a versatile numerical technique to establishing the existence of cavity solitons (CS) in a semiconductor microresonator with bulk GaAs or multiple quantum well GaAs/AlGaAs as its active layer. Based on a Newton method, our approach implies the evaluation of the linearized operator describing deviations from the exact stationary state. The eigenvalues of this operator determine the dynamical stability of the CS. A typical eigenspectrum contains a zero eigenvalue with which a ''neutral mode'' of the CS is associated. Such neutral modes are characteristic of models with translational symmetry. All other eigenvalues typically have negative real parts large enough to cause any excitations to die out in a few medium response times. The neutral mode thus dominates the response to external random or deterministic perturbations, and its excitation induces a simple translation of the CS, which are thus stable and robust. We show how to relate the speed with which a CS moves under external perturbations to the projection of the perturbations on to the neutral mode, and give some examples, including weak gradients on the driving field and interaction with other CS. Finally, we show that the separatrix between two stable coexisting solutions: the homogeneous solution and the CS is the intervening *unstable* CS solution. Our results are important with a view to future applications of CS to optical information processing.

PACS number(s): 42.65.Tg, 05.45.Yv, 42.70.Nq, 45.70.Qj

I. INTRODUCTION

Cavity solitons (CS) have been predicted for a wide variety of nonlinear resonators both in presence [1] and in absence [2] of pattern-forming instabilities [3]. In particular, recent works have shown the possibility of creating and controlling CS in semiconductor microresonators [both multiple quantum well (MQW) and bulk] [4–7]. Results achieved therein pave the way to the application of CS as individually addressable self-organized pixels, suitable for, e.g., reconfigurable arrays, shift registers, and other basic applications for information encoding and processing [8,9]. Nevertheless, theoretical analyses and predictions about CS stability, robustness, and controllability are critical for observation and in particular for their application. The pioneering works for CS in semiconductor microresonators mainly relied their analyses on the direct integration of model equations or on the numerical derivation of the stationary CS profile; the former approach yields just the stable solutions (in particular CS), the latter offers a quantitative criterion to estimate the degree of stability of a stationary solution (e.g., CS belonging to the same branch). As for robustness and controllability, a series of simulations have been performed to appreciate the effect of noise, input field gradients, and of the CS's mutual interaction [5,7]. The aim of this paper is to exploit a different and versatile technique, first applied to saturable absorbing media [8], which allows us to simultaneously assess the existence, the stability, and the dynamical properties of CS in semiconductor microresonators independently from the direct integration of dynamical equations. This method, not unlike the shooting method introduced in [1], yields the system's stationary solutions. Here the transverse Laplacian is evaluated by a fast Fourier transform (FFT). From a suitable initial condition a Newton method is used to find solution(s) to the set of algebraic equations to which the model reduces. There are significant benefits with respect to direct simulation of the partial differential equations (PDE's) describing the full dynamical model. For example, it can yield all the unstable as well as the stable stationary solutions. With respect to the shooting method, it exhibits a much reduced sensitivity to the choice of initial conditions and to the steepness of the solution branches; in addition it is less constrained, and it can yield periodic solutions such as global patterns arising from a modulational instability (MI). Moreover this method has proved generally much more controllable and less computationally demanding. Finally, an important feature of this method is the straightforward derivation of the excitation modes of the CS, both the full eigenspectrum and the relative eigenvector subspace. This is of great relevance with respect to the assessment of CS robustness, mutual interaction properties, and dynamical response to stochastic or deterministic perturbations. The sign of the eigenvalues' real parts, of course, accounts for the CS stability, and a comparison between their relative magnitudes offers an indication about the best operational parameters to optimize CS functionality. The idea is that in order to be considered as particlelike, CS must have all the internal modes well damped; a situation which is shown to occur far from the end points of the stability branch. In common with many transversely unbounded systems, both MQW and bulk models exhibit an eigenspectrum always containing a zero eigenvalue corresponding to the translational invariance of the original equations [8]. By inspecting the spatial profile of the eigenvector associated to the least negative eigenvalue and by following it when the system is brought close to the boundaries of the stable CS branch, one can make predictions on the destabilization pro-

cess which destroys the CS at their existence limits. As for other dynamical properties, a fundamental role is shown to be played by the ''neutral mode,'' i.e., the eigenvector associated to the zero eigenvalue, as has been found already for other different models (e.g., the parametric Ginzburg-Landau model [10]). Interaction of cavity solitons in a degenerate optical parametric oscillator has recently been investigated [11], showing one stable bound state for in-phase CS. On this basis, the interaction properties of CS pairs and the behavior of CS in the presence of phase and/or intensity gradients in the input field profile have been analyzed. We show that the neutral mode dominates the response to perturbations; in particular we give an expression for the CS speed for drifts induced by driving-field gradients; the speed is directly related to the projection of the perturbation onto the neutral mode. Finally, such arguments allow us to interpret the unstable branch of CS as a sort of separatrix between the two different basins of attraction of the homogeneous stationary profile and the stable solitonic solution. The evolution towards either ''attractor'' is dominated by a single unstable mode and therefore the velocity of a CS disappearing or forming can be appreciated ''*a priori*'' with no need, in principle, to lean on a direct simulation. Results obtained in the various instances are always compared to the direct simulation of the model's PDE's, and the agreement is definitely good. For the sake of simplicity we have first developed our model in one dimension (1D), both in Cartesian and cylindrical coordinates; a straightforward 2D extension is unfeasible because the evaluation of a Jacobian for a system of N equations discretized on a grid of $M\times M$ spatial points involves extreme computational efforts. Nevertheless we have investigated also this last situation by introducing some simplifying assumptions. This paper is organized as follows. Section II is devoted to a brief review of the MQW and bulk semiconductor models. Section III contains the description of the numerical method adopted to find stationary solutions and their stability. In Sec. IV we consider the 1D case for two particular range parameters as found in [5,7] and in Sec. V we study the 2D situation exploiting the radial symmetry of CS. The last part of the paper is devoted to the study of CS dynamical properties. In Sec. VI an evolution equation is derived to describe the deviation from stationary solutions due to a perturbation; we derive the expression for the CS speed and study the drift velocity as well as the interaction properties of CS for both MQW and bulk model. The next subsection contains the explanation we gave to the unstable CS branch as a separatrix. Section VII is devoted to conclusions.

II. THE DYNAMICAL EQUATIONS

The system we are considering consists of an optical cavity containing a nonlinear medium and driven by an external coherent field; the nonlinear medium is either a MQW or a bulk sample of GaAs. In the slowly varying envelope approximation and in the mean-field limit the dynamical equations governing the electric field inside the cavity and the carrier density of the active material take the form [5,6]

$$\frac{\partial E}{\partial t}=-(1+\eta+i\,\theta)E+E_I+i\,\Sigma\chi_{nl}E+i\,\nabla_\perp^2 E, \quad (2.1a)$$

$$\frac{\partial N}{\partial t}=-\gamma[N+\beta N^2-\mathrm{Im}(\chi_{nl})|E|^2-d\,\nabla_\perp^2 N], \quad (2.1b)$$

where E and E_I are the normalized slowly varying amplitudes of the intracavity field and external driving field, respectively; θ is the cavity detuning; η is the linear absorption coefficient due to the material in the regions between the semiconductor and the mirrors; Σ is the bistability parameter; N is the carrier density scaled to its transparency value; γ and β are the normalized decay rates of the carrier density that describe the nonradiative and radiative carrier recombination, respectively; d is the diffusion coefficient.

The transverse Laplacian, which describes diffraction in the paraxial approximation, is defined as

$$\nabla_\perp^2=\frac{\partial^2}{\partial x^2}+\frac{\partial^2}{\partial y^2}=\frac{\partial^2}{\partial r^2}+\frac{1}{r}\frac{\partial}{\partial r}+\frac{1}{r^2}\frac{\partial^2}{\partial\phi^2}, \quad (2.2)$$

where (x,y) are Cartesian and (r,ϕ) polar coordinates, in the transverse plane. Below we will consider for simplicity that the driving field E_I is independent of the transverse coordinates, i.e., a plane wave. The results we derive will be approximately valid for cavity solitons supported by an input beam much broader than the individual CS.

The complex susceptibility χ_{nl} describes the nature of the radiation-matter interaction and can be satisfactorily modeled [4–6] for both the MQW and the bulk cases. In MQW structures we consider an optical nonlinearity governed by an excitonic resonance and described *via* a Lorentzian curve. A linear dependence of χ_{nl} on the carrier density N is assumed. The radiation-matter interaction is therefore described by

$$\chi_{nl}(N,\omega_0)=-\frac{1}{\mathrm{Im}(\Theta)}\Theta(N-1) \quad (2.3)$$

with $\Theta=(\Delta+i)/(1+\Delta^2)$; here $\Delta=(\omega_e-\omega_0)/\gamma_e$ is the excitonic detuning, where ω_e and γ_e are the central frequency and the halfwidth of the excitonic line, respectively, and ω_0 is the frequency of the input field. Under this assumption and introducing $C=\Sigma/[2\,\mathrm{Im}(\Theta)]$ Eqs. (2.1a) and (2.1b) recover the original form considered in [4,5].

The case of bulk medium [6,7] is interesting for several reasons. First of all, bulk samples are easier to grow and can be architectured with high accuracy; second, they offer the possibility of high levels of nonlinearity. Nevertheless the model is more complex and numerical simulations more demanding. Adopting the quasiequilibrium approximation the complex susceptibility for the free carriers takes the form

$$\chi_{nl}(N,\omega_0)=-\frac{i}{\epsilon_0\hbar V_A}\sum_{\vec{k}}|\mu_k|^2\frac{f_{ek}(N)+f_{hk}(N)-1}{i(\omega_k-\omega_0)+\gamma_p}, \quad (2.4)$$

where $\vec{k}$ is the carrier momentum, μ_k is the dipole matrix element between the valence and the conduction band (calculated in [13,14]), γ_p is the polarization decay rate (about $10^{13}s^{-1}$), and $\hbar\omega_k=\epsilon_{gap}+\hbar^2k^2/2m_R$ is the transition energy at the carrier momentum k, m_R being the electron-heavy hole reduced mass [15]. V_A is the active volume. The $f_{ek,hk}(N)$ are Fermi-Dirac distributions for electrons and holes, respec-

tively. Two elements are then introduced phenomenologically to properly describe the behavior of the bulk medium in the regimes of interest; one is band-gap renormalization and the other is the Urbach tail. Similarly to the MQW case, we define the band-gap detuning parameter $\Delta=(\omega_{gap}-\omega_0)/\gamma_p$ where ω_{gap} is the band-edge transition frequency and ω_0 is the frequency of the input field. For more details about the bulk model we refer to [6]; at this stage it is worth noting that, with respect to the MQW model, the dependence on N of the bulk susceptibility is highly implicit.

III. STATIONARY SOLUTIONS AND STABILITY

The model consists of three coupled nonlinear time-dependent PDE's, namely Eq. (2.1a), its complex conjugate, and Eq. (2.1b). We opt for $\mathrm{Re}\,E$, $\mathrm{Im}\,E$, and N as our independent variables. In general they are functions of both time and space $(t;x,y)$ but at this stage, we are primarily interested in stationary solutions; $\partial_t E=0=\partial_t N$. Analytical treatment is possible only for the special case of homogeneous stationary solutions, which means to neglect the Laplacian in Eqs. (2.1), but not for more general cases, e.g., cavity soliton solutions. The problem must thus be treated numerically. In what follows we apply a numerical technique, previously applied [8] for a simpler model, to a semiconductor microresonator. For simplicity we describe the technique only in relation to the electric field E although similar considerations apply to the carrier density N.

Consider a square grid $M\times M$ ($M=2^n$ with n integer is best, for efficient use of the fast Fourier transform algorithm); on this grid we discretize the transverse plane (x,y) and consider for each grid point (i,j), with $i,j=1\ldots,M$, the discretized field values $E_{i,j}=E(x_i,y_j)\equiv E(i,j)$. Our first goal is the evaluation of the transverse Laplacian at each grid point, i.e., $(\nabla_\perp^2 E)_{i,j}$. On the assumption of periodic boundary conditions, valid for the models under study for a large enough domain, we numerically evaluate the spatial derivatives using a fast Fourier transform (FFT) algorithm to compute them in Fourier space, where $\nabla_\perp^2\to -k^2$. Thus the spatial second derivatives are numerically evaluated as follows:

$$E(x,y)\to E(i,j)\overset{\mathcal{F}}{\to}\tilde{E}(k_i,k_j)\to -(k_i^2+k_j^2)\tilde{E}\overset{\mathcal{F}^{-1}}{\to}(\nabla_\perp^2 E)_{i,j}, \tag{3.1}$$

where $\mathcal{F}$ denotes Fourier transformation and $\mathcal{F}^{-1}$ denotes back transformation. Starting from the set of values where the variable takes over the whole grid we end with an array that corresponds for each i,j to the transverse Laplacian of the variable at that grid point. After evaluation of all the spatial derivatives, we have at *each* grid point three nonlinear algebraic equations for three variables, all coupled together *via* the transverse Laplacian.

The problem has now been reformulated so that a Newton method can be used to find solution(s) of the nonlinear system. In general, there will be multiple solutions for any given set of parameters, and which one is found by the Newton method depends on the initial conditions supplied. In particular, CS solutions are found from initial isolated peaks of suitable width and amplitude. Once a CS solution is located, it can usually be tracked efficiently in parameter space by using it as input to the system with slightly modified parameters.

The benefit of such a procedure over the more direct simulation of the full time-dependent PDE's is that it can, in principle, yield *all* the stationary solutions, not just those which are dynamically stable. Furthermore, once a stationary solution has been found, its stability can be determined and studied by inspecting the eigenvalues and eigenvectors of the Jacobian matrix obtained by linearizing the system around it. Note that the Jacobian matrix at the stationary solution is needed by the Newton method, and so can be returned as one of its outputs. If any of the eigenvalues of the Jacobian have a positive real part then the solution is unstable. The associated eigenvector gives the spatial profile of the corresponding eigenmode, whether stable, unstable, or neutral. The eigenvector corresponding to an eigenvalue with positive real part will determine the spatial distortion of the unstable solution as the instability develops. Note that the Jacobian and its eigensystem emerge from any Newton method, not just one using the FFT [12].

First, for simplicity we consider a one-dimensional model in which the transverse Laplacian is simply $\nabla_\perp^2=\partial_x^2$ and the discretization process takes place on a line; we refer to Sec. V for the two-dimensional case. On a linear grid of M points we have the following system of $3M$ coupled nonlinear equations:

$$-\overline{\eta}E_r^{(l)}+\theta E_i^{(l)}+E_I^{(l)}-\Sigma[\mathrm{Re}(\chi)^{(l)}E_i^{(l)}+\mathrm{Im}(\chi)^{(l)}E_r^{(l)}] -(\partial_x^2 E_i)^{(l)}=0, \tag{3.2a}$$

$$-\overline{\eta}(E_i)^{(l)}-\theta(E_r)^{(l)}+\Sigma[\mathrm{Re}(\chi)^{(l)}(E_r)^{(l)}-\mathrm{Im}(\chi)^{(l)}(E_i)^{(l)}] +(\partial_x^2 E_r)^{(l)}=0, \tag{3.2b}$$

$$-\gamma[N^{(l)}+\beta N^{(l)2}-\mathrm{Im}(\chi)^{(l)}[(E_r^2)^{(l)}+(E_i^2)^{(l)}]-d(\partial_x^2 N)^{(l)}] =0, \tag{3.2c}$$

where the electric field E has been split into its real E_r and imaginary E_i part; $\overline{\eta}=(1+\eta)$ and $l=1,\ldots,M$ refer to the lth grid point; the $3M$ unknown variables are $E_r^{(l)}$, $E_i^{(l)}$, and $N^{(l)}$.

IV. 1D MODEL

A. MQW

In the following we will analyze the resonant ($\Delta=0$) case for the MQW model; other parameters are $C=30$, $\theta=-3$, $d=0.2$, $\eta=0.25$, $\beta=1.6$, and $\gamma=0.002$. From previous works [5] we already know the expected scenario in two dimensions; in 1D we expect to find again, in almost the same range of values, soliton and roll solutions. The homogeneous steady-state curve is shown in Fig. 1 where solid and dotted line of the S-shaped curve refers to stable and unstable homogeneous solution, respectively. (The stability of the homogeneous solution can be assessed directly by standard techniques, but a Newton method could also be applied to it.) Starting with an initial condition corresponding to a soliton solution as obtained from a direct integration of

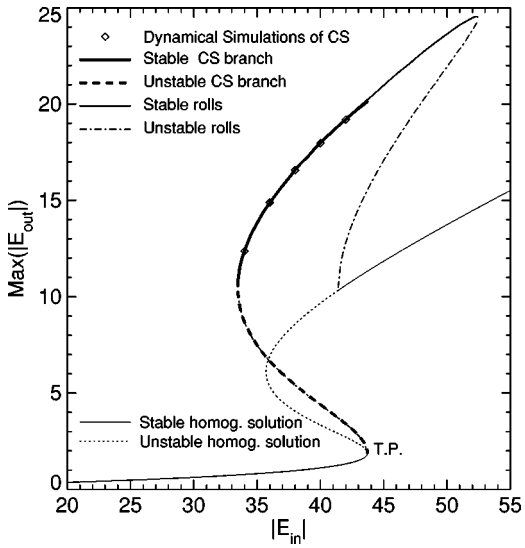

FIG. 1. 1D MQW model. Steady-state curve of the homogeneous solution and results of numerical evaluations and of simulations for cavity soliton and roll stationary solutions. Parameters are $\Delta=0$, $C=30$, $\theta=-3$, $d=0.2$, $\eta=0.25$, $\beta=1.6$, and $\gamma=0.002$. T.P. indicates the turning point of the homogeneous steady-state curve.

Eqs. (2.1) we were able to find a whole branch of stable CS and moreover also an unstable branch. The stable soliton branch is represented in Fig. 1 by a thicker solid line and the unstable branch by a thicker dashed line; as can be seen from Fig. 1 the agreement between the dynamical simulations (diamonds) and the stationary solutions obtained by solving directly the system of nonlinear equations (3.2) is excellent. Thus we have two completely different ways to obtain numerically the CS solutions of our physical system and this reinforces claims that they are not artefacts nor dependent on the particular numerical method. Moreover, the unstable branch, which is found only by our stationary solution approach, gives new insight into the mechanisms that underlie pattern and soliton formation; it is clear from inspection of Fig. 1 that the unstable CS branch bifurcates exactly at the modulational instability (MI) point where the homogeneous solution becomes unstable against pattern formation. (For these particular parameters case MI occurs just at the turning point of the homogeneous steady-state curve).

The stability of CS, as previously mentioned, is readily derived from the solution method used here. We plot as a function of the input intensity in Fig. 2 some of the perturbation eigenvalues of the CS, to be precise the six most ''dangerous'' i.e., the least-negative eigenvalues. The negative-slope branch is characterized throughout its existence range by the presence of a single eigenvalue with positive real part. Note that both branches always exhibit a zero eigenvalue, i.e., a *neutral mode*. This is due to the translational symmetry of the problem. This property is of great importance for applications, as will be discussed below. This neutral mode has an eigenvector which is proportional to the gradient of the CS state itself, because the gradient operator is the generator of translations. In Fig. 3 we have displayed the field E and the carrier density N for a typical soliton solution, their derivatives and the neutral mode $\vec{u}_0$ corresponding to E and N. The close agreement with the exact analytical prediction confirms that discretizing on a finite grid with periodic boundary conditions gives a good approximation to the true problem. As shown in Fig. 2(a), for both decreasing and increasing values of the input field the cavity soliton loses stability when a second eigenvalue approaches zero.

The lower limit corresponds to the turning point at which the upper and lower CS branches merge. It is easy to show that this merger (a *saddle-node bifurcation*) necessarily has an eigenvalue approach zero for each branch. In Fig. 4 we plot the three components of the eigenvector $\vec{u}_1$ which will destabilize the stable cavity soliton at the left end of the branch; both components related to the electric field are highly localized on the cavity soliton and resemble it in shape, while the component corresponding to the the carrier density has a dip at the soliton peak position and two maxima on the sides. Subtracting this mode from the CS will clearly cause it to shrink, and thus this unstable mode can be considered as a switch-off mode (the same way when we use a localized Gaussian beam π out of phase with respect to the background to switch off a CS) [5]. When the input intensity is only slightly increased, it can be seen from Fig. 2 that this mode becomes even more highly damped than the other modes shown. Over the central region of their existence, the CS are thus rather stable. It is worth noting that the magnitude of the largest eigenvalues is comparable to that of γ and this means that any perturbation dies out in a few response times of the medium (which is many cavity response times in our models). Thus all the internal degrees of freedom of these CS are strongly damped, leaving only their translational freedom, giving them a particlelike character.

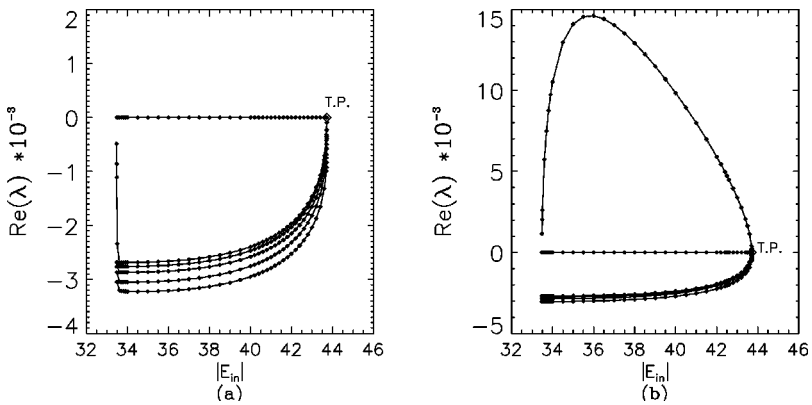

FIG. 2. 1D MQW model. Parameters are as Fig. 1. The six eigenvalues with largest real parts as a function of the input field. (a) Positive-slope (stable) CS branch; (b) Negative-slope (unstable) CS branch. T.P. corresponds to the turning point of the homogeneous steady-state curve.

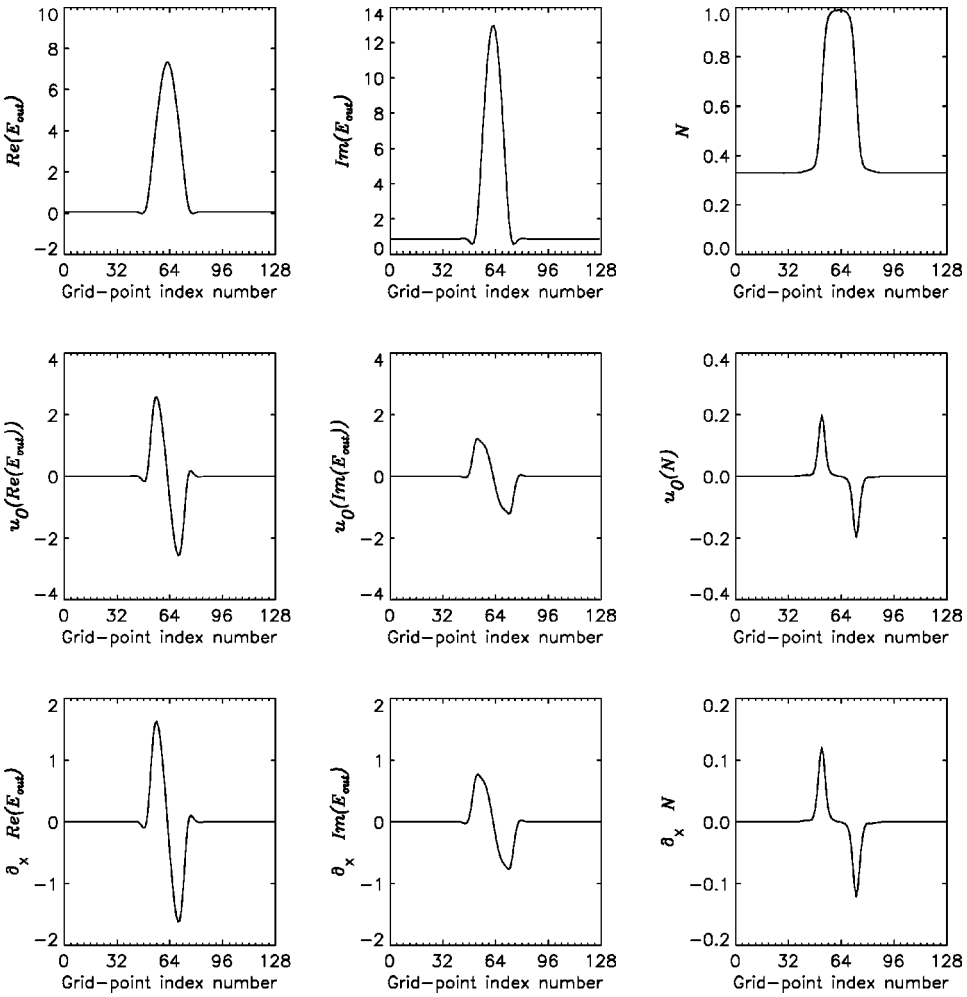

FIG. 3. 1D MQW model. Parameters are as Fig. 1; $|E_I|=38.0$. Top: the real and imaginary part of the electric field and the carrier density relative to a stable CS; Center: the corresponding neutral modes are plotted; Bottom: the calculated derivative of the CS components.

Turning now to the right side of the stable soliton branch, the eigenvector $\vec{u}_1$ that first destabilizes the CS has a completely different shape from the soliton. This is shown in Fig. 5, where we have plotted the three components, as usual, of this eigenvector and for an immediate comparison we have superimposed on the same plot the soliton itself. The destabilizing mode is clearly associated with the homogeneous background, rather than being localizsed on the CS. This is to be expected, since at this end of the branch (high injected fields $|E_I|$) we approach the turning point of the homogeneous steady-state curve and so the CS destabilization can be related to that of the background. This emphasizes that a stable background is a *necessary* condition for a stable cavity soliton. This picture also reinforces the role of the lower-branch homogeneous steady-state solution as a blackboard on which it is possible to ''write'' cavity solitons [4,5]; but a blackboard is an essential prerequisite for such writing. We can examine what happens to a soliton when we increase the value of the input field just slightly above the value corresponding to the turning point. Figure 6 is composed of six frames that show the evolution of the soliton towards a roll pattern. Starting from the unperturbed soliton, the homogeneous solution at the boundary of the grid begins to switch to the upper branch; eventually the soliton can no longer be supported and finally a stable roll pattern emerges. Nevertheless a strong link to the single CS is evidenced by the fact that the minimum and the maximum values of the amplitude of this pattern are very close to those of the single CS, so that the CS can here be regarded as a minimal, self-confined, element of a global pattern. This is also evidenced in Fig. 1

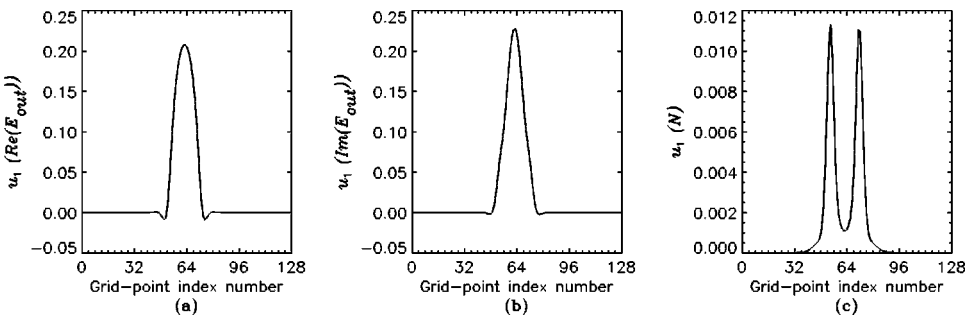

FIG. 4. 1D MQW model. Parameters are as Fig. 1. Eigenvector corresponding to the largest nonzero eigenvalue of the stable CS at $|E_I|=33.476$. (a) and (b) refer, respectively, to the real and imaginary part of the electric field and (c) to the carrier density.

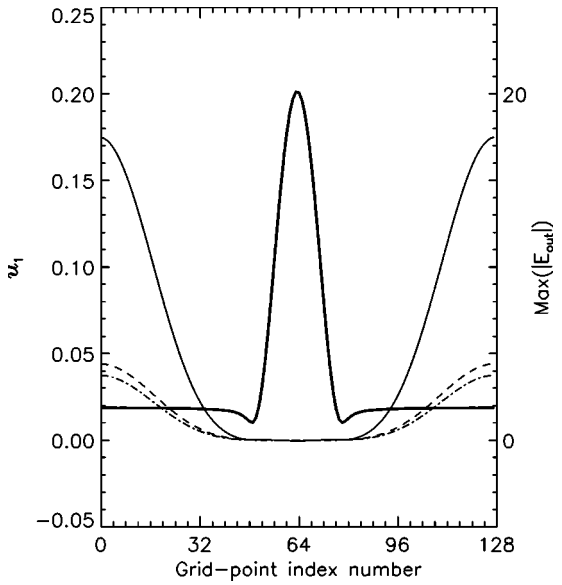

FIG. 5. 1D MQW model. Parameters are as Fig. 1. Eigenvector corresponding to the largest nonzero eigenvalue of the stable CS at $|E_I|=43.72$. Continuous and dotted lines refer, respectively, to the real and imaginary part of the electric field, and dash-dotted line to the carrier density. The thicker line is the cavity soliton. The left ordinate refers to the perturbation mode, the right to the CS.

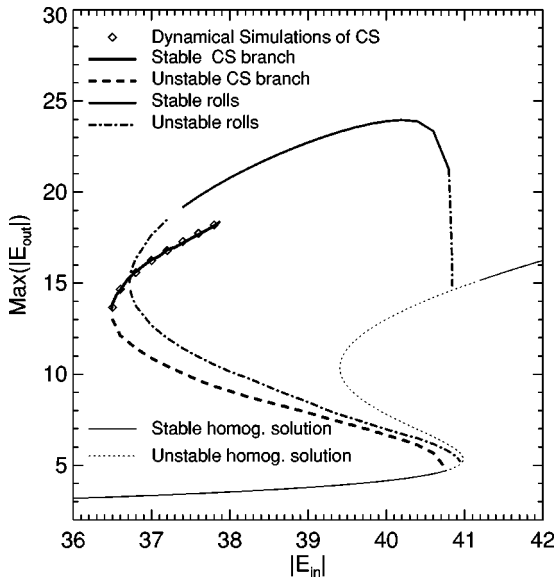

FIG. 7. 1D bulk model. Steady-state curve of the homogeneous solution and results of numerical evaluations and of simulations for cavity soliton and roll stationary solutions. Parameters are $\Delta=1$, $\Sigma=80$, $\theta=-9$, $d=0.2$, $\eta=0$, $\beta=0$, and $\gamma=0.0014$.

where stable and unstable rolls branches are also shown. The 2D counterpart of these multiple localized structures are hexagons, as shown in [5].

B. Bulk

We analyze now the one-dimensional bulk model and in particular we consider the following set of parameters, $\Delta=1$, $\Sigma=80$, $\theta=-9$, $d=0.2$, $\beta=0$, and $\gamma=0.0014$, which have proved to be rather close to experimental conditions [6,7]. The overall picture here is rather different with respect to the MQW case; the lower branch of the homogeneous steady-state solution is no longer entirely stable but a small portion is affected by a modulational instability (MI) close to the turning point (see Fig. 7). More importantly, the shape of the cavity soliton is different; for the bulk model below the bandgap its profile shows damped oscillating tails, not present for the MQW case, and the branch of existence is much more restricted. So the analysis of CS as stationary solutions can give us some insights and possibly link the different shape of solitons to different behaviors.

First, as usual, we compare the results obtained by dynamical simulations to those obtained via direct resolution of the stationary system, and as can be seen from Fig. 7 the agreement is excellent. Following the negative-slope CS branch we find again that the mechanism underlying their

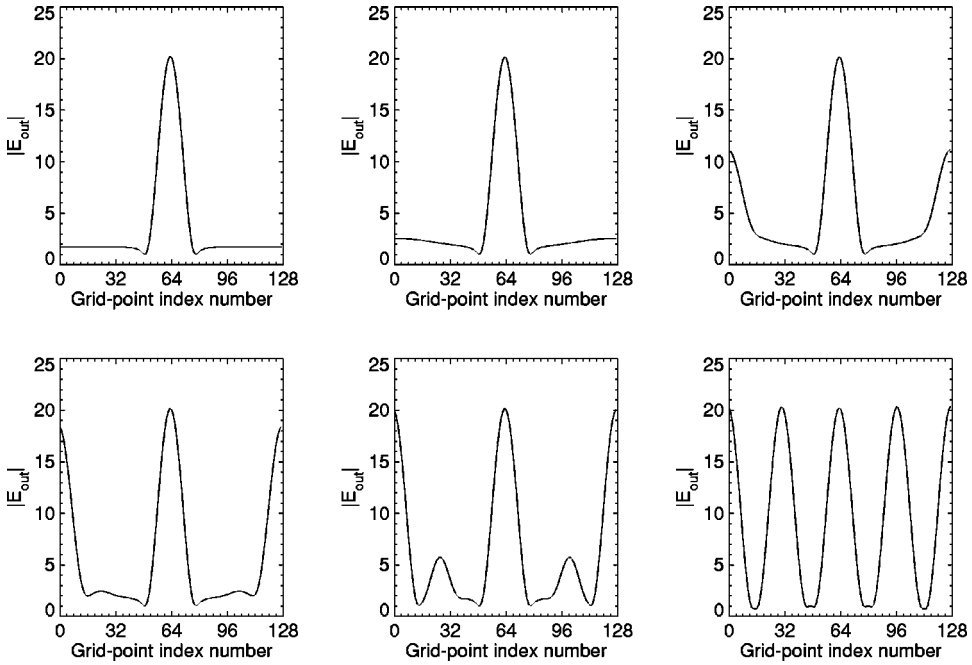

FIG. 6. 1D MQW model. Parameters are as Fig. 1. Six frames corresponding to the evolution (from top-left to bottom-right) of a soliton for $|E_I|=43.8$.

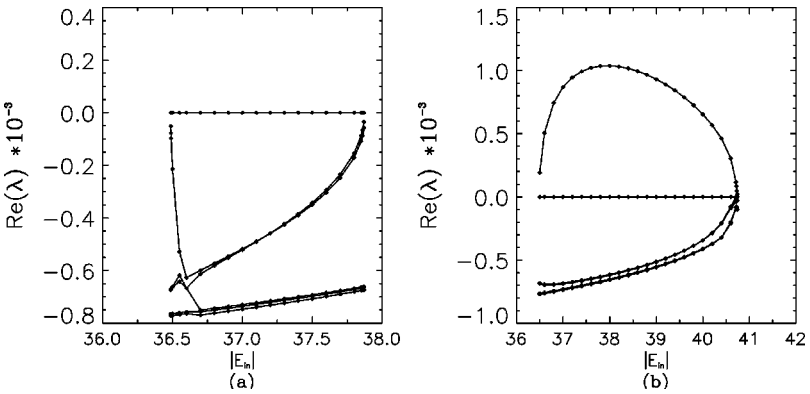

FIG. 8. 1D bulk model. Parameters are as Fig. 7. The six eigenvalues with largest real parts as a function of the input field. (a) Positive-slope (stable) CS branch; (b) Negaitve slope (unstable) CS branch.

existence is linked to MI. In fact the unstable branch connects exactly to the point where the stationary solution becomes modulationally unstable (this is a stronger confirmation than in the MQW case because there the turning point coincides with the onset of MI). We plot as a function of the input intensity in Fig. 8 some of the perturbation eigenvalues of the CS. The negative-slope branch is again characterized by the presence of an eigenvalue with a positive real part, and thus unstable. There always is a zero eigenvalue, again related to translational invariance; on both sides of stable branch a second eigenvalue approaches zero and destabilizes the stationary solution. As done in the MQW case, in Fig. 9 we have displayed for a typical stable CS the field and the carrier density, their derivatives and the neutral mode $\vec{u}_0$.

Let us now examine the mechanisms by which the soliton loses its stability. On the left side of the stable CS branch the picture is as for the MQW model; the first dangerous eigenvector $\vec{u}_1$, the one corresponding to the largest nonzero eigenvalue, has the same field shape of the soliton and the component related to the carrier density presents a dip at the soliton peak position (see Fig. 10). As for the MQW model, over the central region of the stable CS branch the magnitude of the largest eigenvalues is comparable to the value of γ so that the CS are rather stable and almost particlelike.

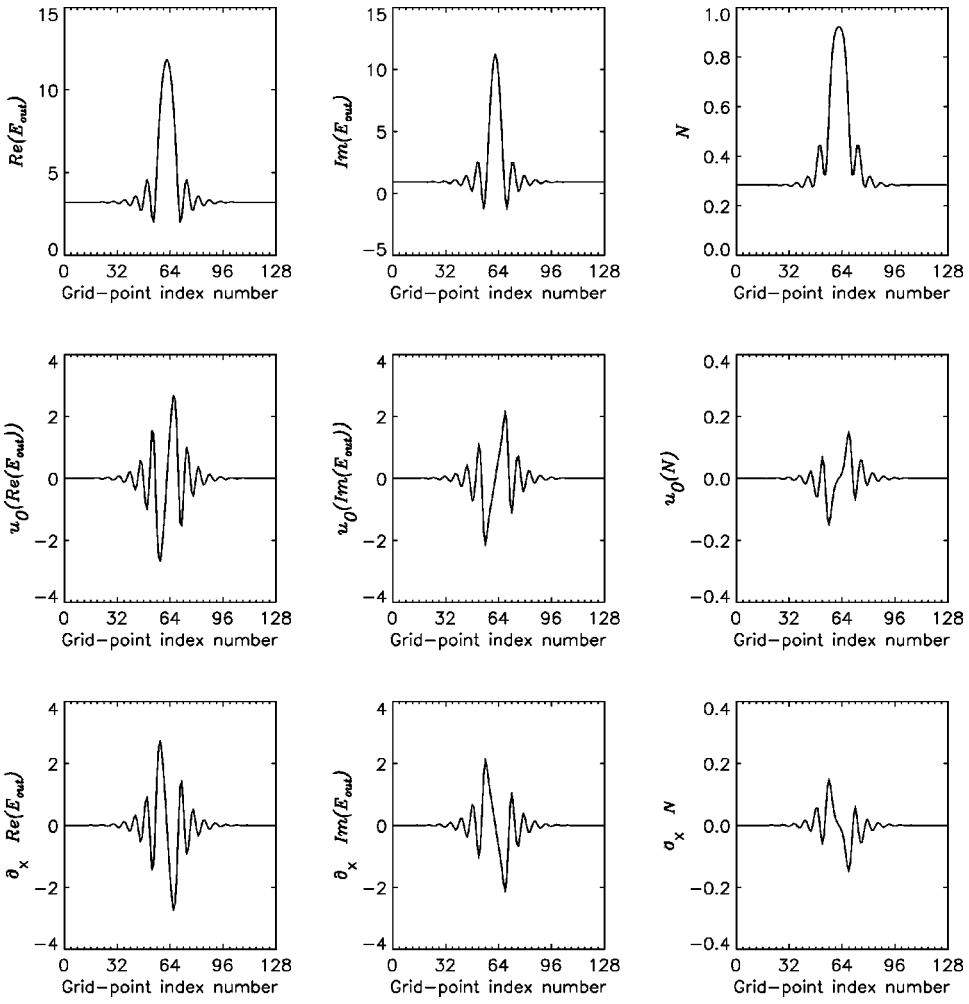

FIG. 9. 1D bulk model. Parameters are as Fig. 7; $|E_I|=37.0$. Top: the real and imaginary part of the electric field and the carrier density relative to a stable CS; Center: the corresponding neutral modes are plotted; Bottom: the calculated derivative of the CS components.

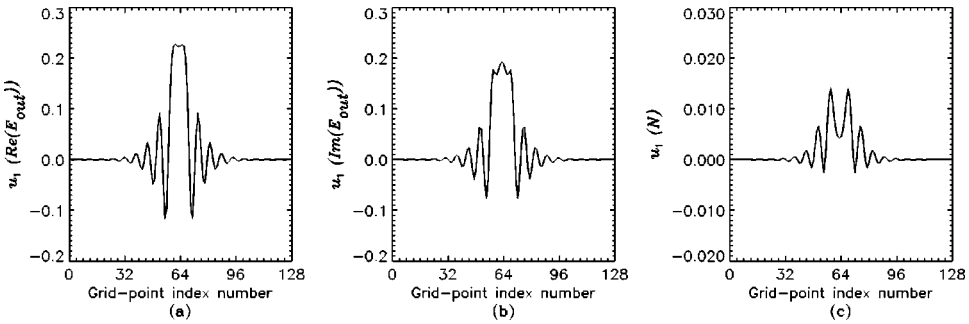

FIG. 10. 1D bulk model. Parameters are as Fig. 7. Eigenvector corresponding to the largest nonzero eigenvalue of the stable CS at $|E_I|=36.488$. (a) and (b) refers, respectively, to the real and imaginary part of the electric field and (c) to the carrier density.

A different situation holds for the right side of the branch, for high input intensity; the first dangerous eigenmode $\vec{u}_1$ reported in Fig. 11 is completely different in shape with respect to MQW model and in this case the destabilization mechanism is clearly localized on the soliton itself. Indeed from Fig. 7 we see that when the upper CS branch terminates there is still a substantial portion of the homogeneous solution branch available as a stable background. The shape of this eigenvector suggests instead that the soliton solution becomes unstable because its subpeaks tend to grow and thus the soliton evolves towards a roll pattern. Indeed this seems to be the case if we look at Fig. 12; here we have reported six frames corresponding to the evolution of an unstable soliton for $|E_I|=38.0$. The side peaks of the soliton grow more and more until a roll solution is reached. Differently from MQW this pattern cannot easily be considered as a multisoliton solution because the minimum value of the field is quite different from the soliton one, and the whole structure is more regular and quasisinusoidal. This is also evidenced in Fig. 7 where stable and unstable rolls branches are also shown. The temporal evolution shown in Fig. 12 suggests that a ''3CS'' state [8] destabilizes the CS, but it is itself unstable so that essentially a switching-wave forms, converting the homogeneous background into a coexisting roll pattern.

V. TWO DIMENSIONAL EXTENSION

The work up to this point is based on a one-dimensional version of the evolution Eqs. (2.1a) and (2.1b) which basically means that we consider only one transverse coordinate. In a two-dimensional extension (2D) a second transverse coordinate has to be considered. With respect to 1D nothing, in principle, changes, we could now simply discretize on a square grid. In practice, this involves a complex Jacobian matrix which is too big to handle. Nevertheless, if we restrict ourselves to radially symmetric solutions, the problem can be simplified; since in polar coordinates (r,ϕ) the solution depends solely on r and not on the angle ϕ. Under this assumption we are again faced with a one-dimensional problem where we discretize in r, and the Jacobian has the same size as in the previous 1D work. Note that the mixed term $(1/r)\times(\partial/\partial r)$ can be evaluated by simply dividing the first derivative, as determined from Fourier space, by r.

The analysis of the MQW model does not present anything new; we have again obtained both stable and unstable branches of solitons and the main difference is that for 2D the soliton's peak intensity is bigger than for 1D. Once more the agreement with the dynamical simulations is excellent. Our 1D findings regarding eigenvalues and eigenvectors similarly extend directly to the 2D case.

For the bulk case some surprises arise, as can be seen from Fig. 13. The soliton branches show a spiraling behavior which suggests possible bistability between solitons of different intensity. We show in the left graph of Fig. 13 the results obtained with the usual stability analysis. According to this, the lower positive-slope branch of the spiral should be stable, but the dynamical simulations show instability. Further, for input fields greater than 38.5 the peak intensity of the soliton decreases until the branch turns back at approximately $|E_I|=39.5$. This portion of soliton branch should be also stable but the dynamical program shows instability for input fields greater than 38.5. This discrepancy with respect to the full 2D dynamical simulation can be easily explained, and agreement restored by an extension of the stability analysis. The Jacobian found in the search for cylindrically symmetric solutions governs radial stability only, i.e., with respect to perturbations which are themselves cylindrically symmetric. We must also, however, consider azimuthally varying perturbations. So let us consider the following form for the perturbation:

$$\varepsilon = R(r) r^{|m|} e^{im\phi}, \tag{5.1}$$

where we allow for an azimuthal dependence *via m*. After some calculations we obtain

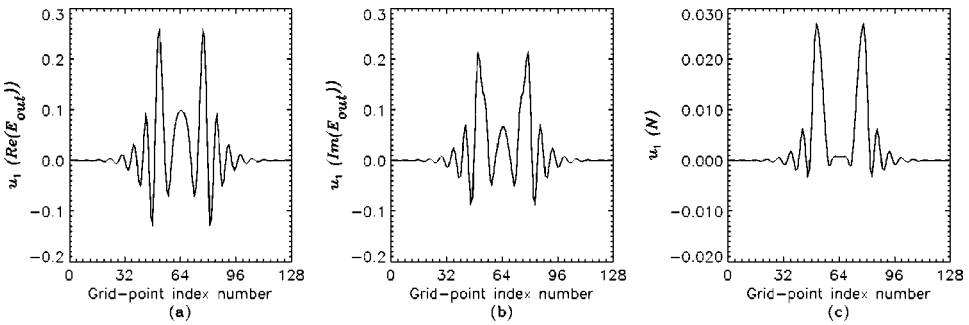

FIG. 11. 1D bulk model. Parameters are as Fig. 7. Eigenvector corresponding to the largest nonzero eigenvalue of the stable CS at $|E_I|=37.87$. (a) and (b) refers, respectively, to the real and imaginary part of the electric field and (c) to the carrier density.

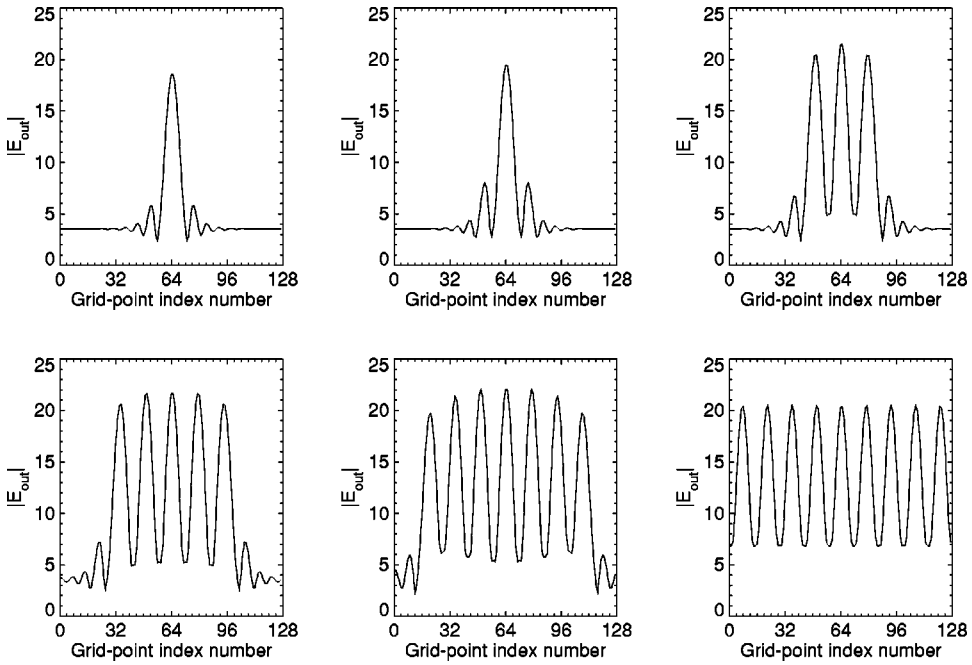

FIG. 12. 1D bulk model. Parameters are as Fig. 7. Six frames corresponding to the evolution (from top-left to bottom-right) of a soliton for $|E_I|=38.0$.

$$\nabla_\perp^2 \varepsilon = \left(\frac{d^2R}{dr^2} + \frac{(2|m|+1)}{r} \frac{dR}{dr} \right) r^{|m|} e^{im\phi}. \qquad (5.2)$$

When we perform the stability analysis all the terms $r^{|m|}e^{im\phi}$ cancel out and the contribution of the transverse Laplacian in Eq. (5.2) to the Jacobian is due only to the term in round brackets. The term $(2|m|+1)$ accounts for azimuthal perturbation; for $m=0$ we recover the usual radial case but for higher values we introduce azimuthal effects which contribute to the the eigenvalues of the Jacobian. We show in Fig. 14 what happens to the eigenvalues for different values of m. Starting from the left we have $m=0$ that correspond to purely radial perturbations, with only negative eigenvalues. Next we have the case $m=\pm 1$ where there is a neutral mode; it is easy to show this is again associated with the translational symmetry. Finally, we have the case $m=\pm 2$ and we see that for this value the upper CS branch loses its stability exactly at 38.5 according to the dynamical simulations. In Fig. 15 we report six frames of a dynamical simulation which show the destabilization of a cavity soliton for an input value of the field slightly above 38.5. It clearly exhibits instability *via* an asymmetric deformation of $m=2$ type. The eventual roll structure is influenced by the periodic boundary conditions, but the onset of the instability should be accurately portrayed. Finally, note that the band of negative eigenvalues with values in the range $-1.0<\lambda<-0.5$ looks almost the same for each m. This shows that these are indeed background modes, insensitive to the phase profile at the soliton core.

VI. RESPONSE TO PERTURBATIONS

Next we analyze the effect of perturbations on the stable CS solutions described so far. In view of possible applications to optical processing schemes this response merits investigation. As we shall see the eigenvalues and eigenvectors of the CS Jacobian again play an important role.

Let us write the system equations in the concise vectorial form

$$\frac{\partial \vec{E}}{\partial t} = \vec{f}(\vec{E}) + \vec{E}_I, \qquad (6.1)$$

where $\vec{E}$ is the vector of *all* unknown variables, $\vec{f}$ is a generic nonlinear function, and $\vec{E}_I$ is the vector which describes the driving field(s). We have to consider two different types of perturbation and treat them in a slightly different way. Namely *external* perturbations of the driving field (they could be due to noise as well as imposed amplitude or phase perturbation of the input fields), and *internal* perturbations which are related directly to the dependent variables and enter into the evaluation of the nonlinear function $\vec{f}$. These last

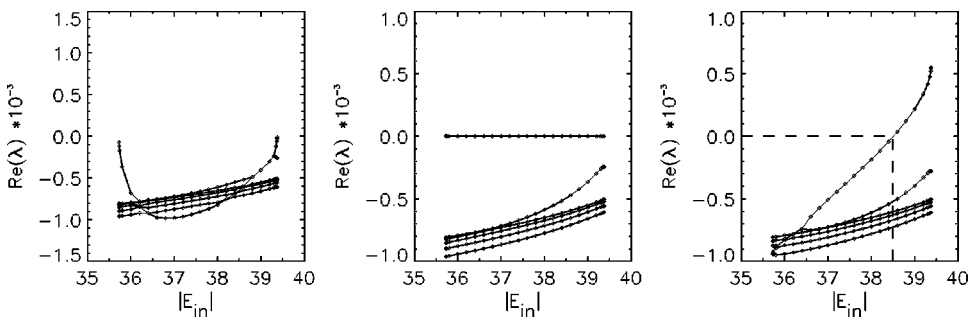

FIG. 13. 2D bulk model. Parameters are as Fig. 7. Stability assignations on the left refer to purely radial perturbations, those on the right include azimuthal perturbations also. The dynamical simulations agree only with the latter.

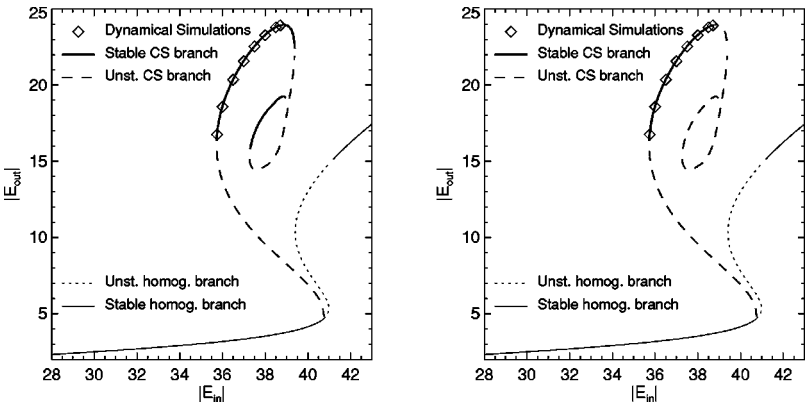

FIG. 14. 2D bulk model. Parameters are as Fig. 7. Perturbation eigenvalues as a function of the input field for the upper CS branch of Fig. 13. The perturbations are of the form (5.1) with azimuthal indices: $m=0$ (left); $|m|=1$ (center); $|m|=2$ (right).

correspond to fluctuations in the values of parameters such as θ as well as to perturbations due to interactions between cavity solitons.

External perturbation. Let $\vec{E}_S$ be a stationary solution $\Rightarrow \partial\vec{E}_S/\partial t=0=\vec{f}(\vec{E}_S)+\vec{E}_I$ and consider a small perturbation on the external driving field

$$\frac{\partial\vec{E}}{\partial t}=\vec{f}(\vec{E})+\vec{E}_I+\vec{P}_{ext}. \tag{6.2}$$

Due to the perturbation the solution suffers a slight deviation from the stationary value and can be written as $\vec{E}=\vec{E}_S+\vec{\varepsilon}$; inserting this into Eq. (6.2) we obtain

$$\frac{\partial\vec{\varepsilon}}{\partial t}=\vec{f}(\vec{E}_S)+\left(\frac{d\vec{f}}{d\vec{E}}\right)_{\vec{E}_S}\vec{\varepsilon}+\vec{E}_I+\vec{P}_{ext}=\mathbf{J}_S\cdot\vec{\varepsilon}+\vec{P}_{ext}, \tag{6.3}$$

where $\mathbf{J}_S$ is the Jacobian of the stationary solution (exactly as used in the Newton solution method).

Internal perturbation. In this case the perturbation is related to the intracavity field itself and so we need to consider its effect on the evaluation of the nonlinear function $\vec{f}$;

$$\frac{\partial\vec{E}}{\partial t}=\vec{f}(\vec{E}+\vec{P}_{int})+\vec{E}_I, \tag{6.4}$$

nevertheless we assume again that $\vec{E}=\vec{E}_S+\vec{\varepsilon}$. With this assumption the evolution equation for $\vec{\varepsilon}$ becomes

$$\frac{\partial\vec{\varepsilon}}{\partial t}=\vec{f}(\vec{E}_S)+\left(\frac{d\vec{f}}{d\vec{E}}\right)_{\vec{E}_S}(\vec{\varepsilon}+\vec{P}_{int})+\vec{E}_I=\mathbf{J}_S\cdot(\vec{\varepsilon}+\vec{P}_{int}). \tag{6.5}$$

Thus in both cases it is possible to write the same form of evolution equation for the deviation from the stationary solution:

$$\frac{\partial\vec{\varepsilon}}{\partial t}=\mathbf{J}_S\cdot\vec{\varepsilon}+\vec{\mathcal{P}}. \tag{6.6}$$

At this point we assume that $\vec{\varepsilon}$ can be expressed in terms of the basis $\{\vec{u}_i\}$ formed by the eigenvectors of the Jacobian,

$$\vec{\varepsilon}=\sum_j a_j|\vec{u}_j\rangle \quad \text{where} \quad \mathbf{J}_S|\vec{u}_j\rangle=\lambda_j|\vec{u}_j\rangle$$

and Eq. (6.6) becomes

$$\sum_j \frac{da_j}{dt}|\vec{u}_j\rangle=\mathbf{J}_S\sum_j a_j|\vec{u}_j\rangle+\vec{\mathcal{P}}. \tag{6.7}$$

To further analyze Eq. (6.7) we recall and apply the concept of biorthogonality. Let $\mathbf{J}_S^T$ be the transposed matrix of $\mathbf{J}_S$ and

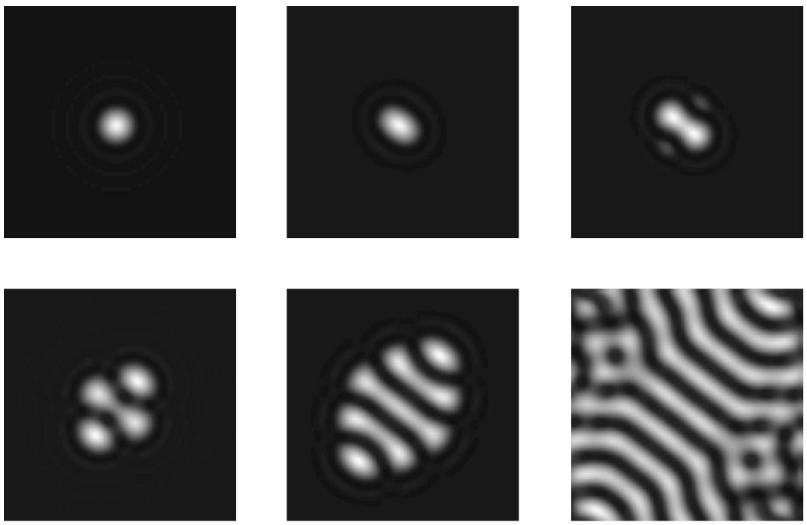

FIG. 15. 2D bulk model. Parameters are as Fig. 7. Dynamical evolution of a soliton solution for input field $|E_I|=38.6$; starting from the top left it is possible to see how the soliton destabilizes via an azimuthal instability.

let $\langle \vec{v}_j | \mathbf{J}_S^T = \langle \vec{v}_j | \zeta_j$; it can be shown that $\lambda_j = \zeta_j$ and that, when properly normalized, $\langle \vec{v}_i | \vec{u}_j \rangle = \delta_{ij}$. These relations expresses the biorthogonality properties of eigenvectors of operators which are not self-adjoint. We can project both sides of Eq. (6.7) on $\langle \vec{v}_i |$ and exploit the biorthogonality relation obtaining:

$$\langle \vec{v}_i | \vec{u}_i \rangle \frac{da_i}{dt} = \langle \vec{v}_i | \vec{u}_i \rangle \lambda_i a_i + \langle \vec{v}_i | \vec{\mathcal{P}} \rangle \Rightarrow \tag{6.8}$$

$$\frac{da_i}{dt} = \lambda_i a_i + \frac{1}{\langle \vec{v}_i | \vec{u}_i \rangle} \langle \vec{v}_i | \vec{\mathcal{P}} \rangle. \tag{6.9}$$

For generality, we have not normalized the vector basis.

It is reasonable to assume that $\forall i \;\; a_i(t=0)=0$ which physically means that when the perturbation is turned on, the corresponding deviation from the stationary solution begins to grow from zero. With this initial condition we obtain the following expressions for the perturbation coefficients a_i:

$$a_i(t) = \frac{1}{\lambda_i} \frac{\langle \vec{v}_i | \vec{\mathcal{P}} \rangle}{\langle \vec{v}_i | \vec{u}_i \rangle} (e^{\lambda_i t} - 1) \quad \text{if} \quad \lambda_i \neq 0, \tag{6.10}$$

$$a_0(t) = \frac{\langle \vec{v}_0 | \vec{\mathcal{P}} \rangle}{\langle \vec{v}_0 | \vec{u}_0 \rangle} t \quad \text{for} \quad \lambda = 0. \tag{6.11}$$

Evidently for long times ($t \to \infty$) the behavior of each a_i strongly depends upon the corresponding eigenvalue λ_i. Provided $\vec{E}_S$ is a stable stationary solution, all the eigenvectors except $|\vec{u}_0\rangle$ have eigenvalues with negative real part. This means that, as $t \to \infty$, a_0 dominates over all other a_i. Thus the effect of any perturbation on a stationary stable state is essentially determined by its overlap with the neutral mode of the transposed matrix of the Jacobian. Thus we need only consider the rather simple equation

$$\frac{da_0}{dt} = \frac{1}{\langle \vec{v}_0 | \vec{u}_0 \rangle} \langle \vec{v}_0 | \vec{\mathcal{P}} \rangle. \tag{6.12}$$

Now, the physical meaning af da_0/dt is the velocity of the CS under the influence of the perturbation. To see this, note that after a transient the perturbation of the stationary stable solution is simply $\vec{\varepsilon} = a_0 |\vec{u}_0\rangle$ so that $\vec{E} = \vec{E}_S + a_0 |\vec{u}_0\rangle$; recall now from Sec. IV that the neutral mode is proportional to the gradient of the solution itself, i.e., (in 1D for simplicity):

$$|\vec{u}_0\rangle = \alpha \frac{d\vec{E}_S}{dx} \Rightarrow \vec{E} = \vec{E}_S + a_0 \alpha \frac{d\vec{E}_S}{dx}. \tag{6.13}$$

Consider now a soliton slightly displaced from its initial position x_0 and perform a first-order expansion around x_0:

$$\vec{E}_S(x_0 + \xi) = \vec{E}_S(x_0) + \xi \frac{d\vec{E}_S(x_0)}{dx}. \tag{6.14}$$

From a direct comparison of Eqs. (6.13) and (6.14) we see that $\xi = a_0 \alpha$ and this implies that the velocity v of the soliton is

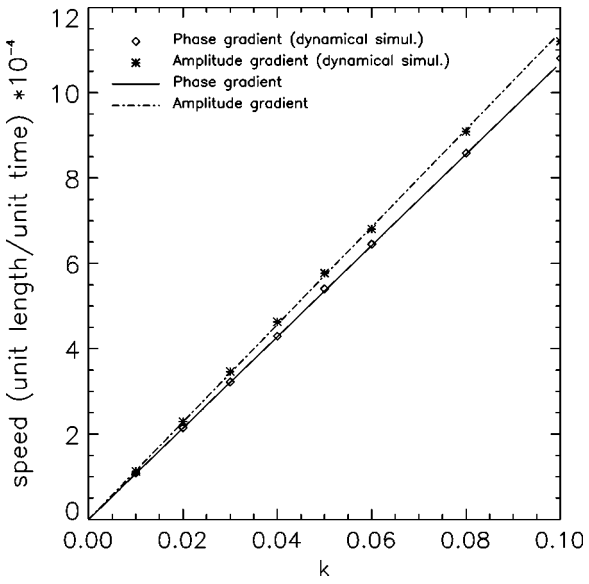

FIG. 16. 1D MQW model. Parameters are as Fig. 1. CS drift velocity vs gradient coefficient k. Solid and dash-dotted lines refer to phase gradient and amplitude gradient, respectively. Diamonds and stars refer to evaluation of CS drift velocity in a corresponding dynamical simulation. For a typical microresonator 1 unit length/unit time $\approx 35 \times 10^4$ μm/μs.

$$v = \frac{d\xi}{dt} = \frac{da_0}{dt} \alpha = \alpha \frac{\langle \vec{v}_0 | \vec{\mathcal{P}} \rangle}{\langle \vec{v}_0 | \vec{u}_0 \rangle} = \frac{\langle \vec{v}_0 | \vec{\mathcal{P}} \rangle}{\left\langle \vec{v}_0 \middle| \frac{d\vec{E}_S}{dx} \right\rangle}. \tag{6.15}$$

So we have shown that only the projection of the perturbation on the neutral mode is relevant for the dynamics of CS; moreover the neutral mode is an odd function of x and so, as a further restriction, only the odd component of any perturbation is important.

Among the various types of perturbations, we analyze three of particular relevance. Two are external perturbations, a phase gradient and an amplitude gradient in the driving field. The other is internal, perturbation of a soliton with respect to another soliton.

In the case of a phase gradient imposed on the homogeneous background $E_I^{(h)}$ the input field takes the following form:

$$E_I(x) = E_I^{(h)} e^{ikx} \simeq E_I^{(h)}(1 + ikx), \tag{6.16}$$

where the last relation holds for kx sufficiently small; then the perturbation is $\vec{\mathcal{P}} = E_I^{(h)} ikx$. Similarly an amplitude gradient yields $\vec{\mathcal{P}} = E_I^{(h)} kx$. Inserting these perturbations into Eq. (6.15) we can calculate the drift velocity of a CS in the presence of a weak phase or amplitude gradient on the input field. In Figs. 16 and 17 we show the results for the MQW and the bulk model, respectively; in both cases the agreement with a direct evaluation of the drift velocity *via* dynamical simulations is extremely good. Now consider the perturbation of a soliton with respect to another soliton. Let $\vec{E}_1$ represent the first soliton, located at x_1, and $\vec{E}_2$ the second, at x_2, where $|x_2 - x_1|$ is large enough compared to the soliton width, so that the effect of $\vec{E}_2$ at the location x_1 can

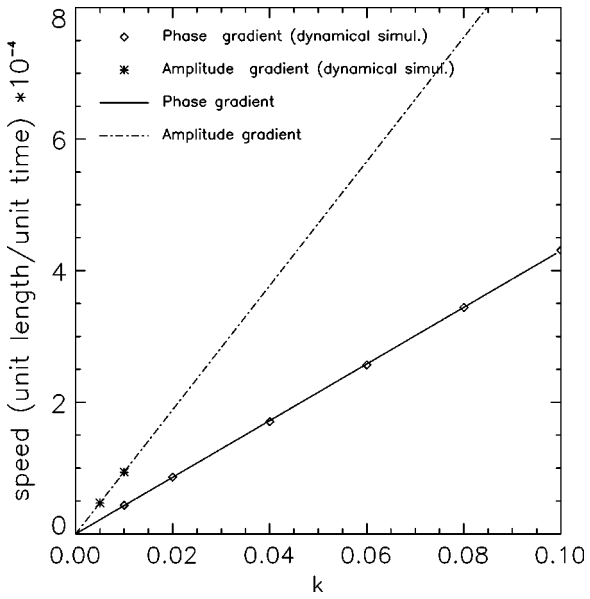

FIG. 17. 1D bulk model. Parameters are as Fig. 7. Otherwise as Fig. 16.

be considered a small perturbation to $\vec{E}_1$. Being an internal perturbation, in this case we have $\vec{\mathcal{P}}=\mathbf{J}_1\cdot\vec{E}_2$; inserting this into Eq. (6.15) we can calculate the velocity of the first soliton induced by the second one. By symmetry, the relative velocity is twice this. Note that the interaction ''force'' governs the relative velocity, not the relative acceleration. Any separation distance at which the mutual perturbation vanishes is thus a ''bound state'' of the two CS (maybe an unstable one). In Figs. 18 and 19 we report the results obtained in the MQW and in the bulk model, respectively. By convention the relative velocity is negative for two solitons moving apart, positive for the opposite case.

For the MQW case no equilibrium distance is predicted; two solitons should either attract each other or should have negligible interaction. But in fact dynamical simulations have shown that there is actually one equilibrium position, while two CS are effectively independent when their reciprocal distance is greater than 50 grid points. So the perturbation method predicts quite well the noninteraction distance but fails to predict the bound state. In the bulk model the situation is more complicated; as can be seen from Fig. 19 there are several interequilibrium distances, indicated with stars and diamonds. But, contrary to the MQW case, here the method is very predictive and we were able to find *via* direct dynamical simulations all the bound states marked with stars. For each of these, a change of separation results in a relative velocity of opposite sign, so the stability of these bound states is also correctly predicted. The two zeroes marked with diamonds do not correspond to stable bound states: here the two solitons are themselves unstable and evolve towards a roll solution.

Separatrix

An important result concerning the role of the unstable CS branch acting as a separatrix can be obtained exploiting the considerations developed so far. We recall that the dynamics of the unstable CS, both in MQW and in bulk model, is governed by a single eigenmode, with an eigenvector whose shape is not dissimilar from the unstable soliton. Being essentially a single-mode behavior we can anticipate that the locus of the unstable CS will act as a separatrix of the two stable coexisting solutions: the homogeneous solution and the CS. Dynamical simulations confirm this role for both MQW and bulk, in both 1D and in 2D; to check this we have initialized with an unstable soliton. If we just slightly increase the input field then the field evolves towards a stable soliton, while if we slightly decrease the input field it decays to the homogeneous background.

This behavior follows from the perturbation response of the unstable soliton, since, according to Eq. (6.11), the mode amplitude that prevails is the one related to the eigenvector with positive eigenvalue, thus

$$a_+(t)\sim\frac{\langle\vec{v}_+|\vec{\mathcal{P}}\rangle}{\langle\vec{v}_+|\vec{u}_+\rangle}t, \tag{6.17}$$

where + refers to the single unstable mode. The perturbed solution can be written as follows:

$$\vec{E}=\vec{E}_S+\vec{\varepsilon}\sim\vec{E}_S+a_+|\vec{u}_+\rangle=\vec{E}_S+\frac{\langle\vec{v}_+|\vec{\mathcal{P}}\rangle}{\langle\vec{v}_+|\vec{u}_+\rangle}t|\vec{u}_+\rangle. \tag{6.18}$$

The shape of $|\vec{u}_+\rangle$ is very similar to that of the soliton itself, and so it will act as a switch-off or a switch-on agent according to the sign of the coefficient. Considering $\vec{\mathcal{P}}$ as a slight deviation from the input field, our checks show that an increase in the input field correspond to a positive sign, while a decrease to a negative sign, thus confirming the role of the unstable branch as a separatrix. Our analysis also shows that

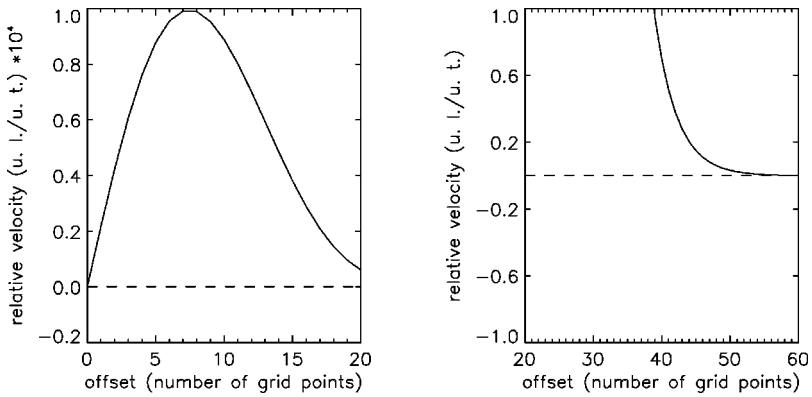

FIG. 18. 1D MQW model. Parameters are as Fig. 1. Interaction of two cavity solitons at $|E_I|=38.0$. Half width at hal maximum (HFHM) of a CS is 15 grid points. *x* axis: their separation in terms of number of grid points. *y* axis: relative velocity of the solitons (negative when moving apart, units arbitrary). For a typical microresonator 1 unit length (u. l.)/unit time (u. t.) $\approx 35\times10^4$ μm/μs.

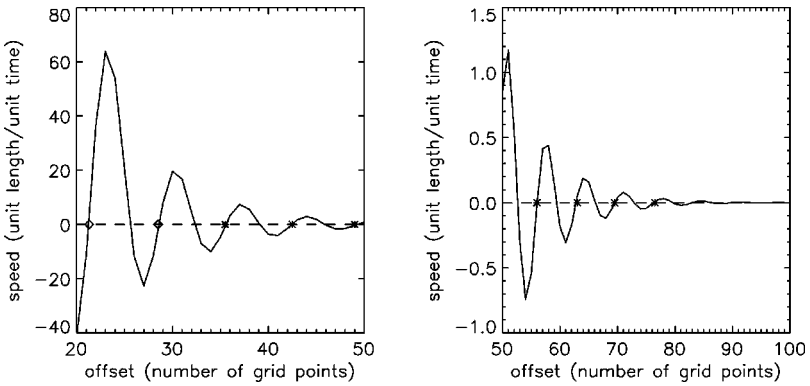

FIG. 19. 1D bulk model. Parameters are as Fig. 7. Interaction of two cavity solitons at $|E_I| = 37.0$. HFHM of a CS is 10 grid points. Otherwise as Fig. 18.

the unstable soliton is in fact *metastable*, in that it is an attractor for all nearby states except those proportional to its single unstable mode. Address pulses will thus spontaneously reshape themselves into the shape of the unstable soliton (if ''nearby''), before evolving away along its unstable manifold, either to the stable CS or to the flat solution.

In addition we have checked that the evolution of an unstable soliton towards a stable soliton has a temporal behavior proportional to $(e^{\lambda_+ t}-1)$ where λ_+ is the eigenvalue of the unstable mode; this occurs up to a time scale long compared to $1/\lambda_+$ and is in accordance with Eq. (6.10). The same happens when the unstable soliton evolves towards the homogeneous solution.

VII. CONCLUSIONS

In this work we have applied a seminumerical method developed on fairly simple nonlinear optical models [8] to investigate cavity soliton properties in a semiconductor microresonator with a bulk GaAs or MQW GaAs/AlGaAs active layer. This approach not only allows us to find the stationary solutions, including CS, as the method adopted in [5,7] did, but as a valuable improvement also returns the eigenvalue spectrum and associated eigenvectors, derived from the analysis of the Jacobian of the nonlinear system (3.2). On this basis, the stability properties of the CS have been thoroughly described. The method is in fact applicable to any type of stationary solution, as forthcoming communications will illustrate. The overall indications—by analyses based on independent approaches—about the existence of stable CS, their shape and relations with the global structures arising from the modulational instability, have thus been strengthened by the study of the eigenvalue spectrum, exploiting the role of the neutral mode and evidencing best ranges for CS stability. The CS can be said to be stronger where their internal eigenmodes are most strongly damped. Moreover, a straightforward extension of the method to 2D revealed the role of azimuthally asymmetric perturbations. Indeed the CS dynamics and stability appears governed by mechanisms whose simplification to one spatial dimension implies some loss of information, and our works proceed toward a full 2D implementation of the method. A further important result of the Newton approach is its capability of predicting the effect of perturbations on the CS dynamics which is ruled by the unstable, neutral, or weakly damped modes, according to the particular conditions. We derived some helpful indications concerning possible applications of CS to optical information processing. The imposition of a gradient in the input field (amplitude or phase), has been shown to induce a drifting dynamics ruled by the neutral mode associated to translations. The CS speed across the device section can be calculated *a priori* using perturbation methods, in good agreement with the simulation approach previously adopted [7]. Also, a relevant indication is the fact that the short/middle-term dynamics of the unstable CS is governed by a single unstable eigenmode. Our analysis indicates that the locus of the unstable CS is actually a subspace projection of the basin of attraction—in principle very complex—of the two stable coexisting solutions: the homogeneous solution and the CS. This indication can be translated into an *a priori* prediction about the address pulse characteristics, e.g., power and duration, when CS must be written and erased.

ACKNOWLEDGMENT

This study was carried out within the framework of the ESPRIT LTR Project PIANOS (*Processing of Information by Arrays of Nonlinear Optical Solitons*).

[1] W.J. Firth and A.J. Scroggie, Phys. Rev. Lett. **76**, 1623 (1996).
[2] N.N. Rosanov, Prog. Opt. **35**, 1 (1996).
[3] L.A. Lugiato, M. Brambilla, and A. Gatti, in *Advances in Atomic, Molecular and Optical Physics*, edited by B. Bederson and H. Walther (Academic, New York, 1998), Vol. 40, p. 229; F.T. Arecchi, S. Boccaletti, and P. Ramazza, Phys. Rep. **318**, 1 (1999).
[4] M. Brambilla *et al.*, Phys. Rev. Lett. **79**, 2042 (1997).
[5] L. Spinelli, *et al.*, Phys. Rev. A **58**, 2542 (1998).
[6] G. Tissoni, *et al.*, J. Opt. Soc. Am. B **16**, 2083 (1999).
[7] G. Tissoni, *et al.*, J. Opt. Soc. Am. B **16**, 2095 (1999).
[8] W.J. Firth and G.K. Harkness, Asian J. Phys. **7**, 665 (1998).
[9] W.J. Firth, Proc. SPIE **4016**, 388 (2000).
[10] S. Longhi, Phys. Rev. E **55**, 1060 (1997).
[11] D.V. Skryabin and W.J. Firth, Opt. Lett. **24**, 1056 (1999).
[12] U. Peschel *et al.*, Phys. Rev. E **58**, R2745 (1998).

[13] G.P. Bava, P. Debernardi, and A. Pisoni, *QW Optical Response Including Valence Band Mixing and Many Body Effects*, Internal Rep. DE/GE 91–002 (Politecnico di Torino, Turin, Italy, 1993).

[14] K.W. Boer, *Survey of Semiconductor Physics* (Van Nostrand Reinhold, New York, 1990).

[15] W.W. Chow, S.W. Koch, and M. Sargent III, *Semiconductor-Laser Physics* (Springer-Verlag, Berlin, 1994).